Research Article | Vol. 24, No. 23 | 14 Nov 2016 | OPTICS EXPRESS 26464
Optics EXPRESS

Mid infrared quantum cascade laser operating in pure amplitude modulation for background-free trace gas spectroscopy

YVES BIDAUX,[1,*] ALFREDO BISMUTO,[2] PIETRO PATIMISCO,[3,4] ANGELO SAMPAOLO,[3,4] TOBIAS GRESCH,[2] GREGORY STRUBI,[2] STÉPHANE BLASER,[2] FRANK K TITTEL,[3], VINCENZO SPAGNOLO,[4] ANTOINE MULLER,[2] AND JÉRÔME FAIST,[1]

[1]*Institute for Quantum Electronics, ETH-Zurich, CH-8093 Zurich, Switzerland*
[2]*Alpes Lasers SA, Avenue des Pâquiers 1, CH-2072 Saint-Blaise, Switzerland*
[3]*Department of Electrical and Computer Engineering, Rice University, 6100 Main Street, Houston, TX 77005, USA*
[4]*Dipartimento Interateneo di Fisica, University and Politecnico of Bari, CNR-IFN UOS BARI, Via Amendola 173, Bari 70100, Italy*
[*]*bidauxy@phys.ethz.ch*

Abstract: We present a single mode multi-section quantum cascade laser source composed of three different sections: master oscillator, gain and phase section. Non-uniform pumping of the QCL's gain reveals that the various laser sections are strongly coupled. Simulations of the electronic and optical properties of the laser (based on the density matrix and scattering matrix formalisms, respectively) were performed and a good agreement with measurements is obtained. In particular, a pure modulation of the laser output power can be achieved. This capability of the device is applied in tunable-laser spectroscopy of N_2O where background-free quartz enhanced photo acoustic spectral scans with nearly perfect Voigt line shapes for the selected absorption line are obtained.

© 2016 Optical Society of America

OCIS codes: (140.5965) Semiconductor lasers, quantum cascade; (230.1480) Bragg reflectors; (250.5960) Semiconductor lasers; (140.0140) Lasers and laser optics.

References and links

1. J. Faist, F. Capasso, D. L. Sivco, C. Sirtori, A. L. Hutchinson, and A. Y. Cho, "Quantum Cascade Laser," Science **264**, 553–556 (1994).
2. Y. Bai, N. Bandyopadhyay, S. Tsao, S. Slivken, and M. Razeghi, "Room temperature quantum cascade lasers with 27% wall plug efficiency," Applied Physics Letters **98**, 181102 (2011).
3. A. Bismuto, Y. Bidaux, S. Blaser, R. Terazzi, T. Gresch, M. Rochat, A. Muller, C. Bonzon, and J. Faist, "High power and single mode quantum cascade lasers," Optics Express **24**, 10694 (2016).
4. A. Bismuto, S. Blaser, R. Terazzi, T. Gresch, and A. Muller, "High performance, low dissipation quantum cascade lasers across the mid-IR range," Optics Express **23**, 5477 (2015).
5. A. Kosterev, G. Wysocki, Y. Bakhirkin, S. So, R. Lewicki, M. Fraser, F. Tittel, and R. Curl, "Application of quantum cascade lasers to trace gas analysis," Applied Physics B **90**, 165–176 (2008).
6. C. K. N. Patel, "Quantum cascade lasers: a game changer for defense and homeland security IR photonics," in "SPIE Defense, Security, and Sensing," (International Society for Optics and Photonics, 2011), pp. 803126.
7. K. Ruxton, A. Chakraborty, W. Johnstone, M. Lengden, G. Stewart, and K. Duffin, "Tunable diode laser spectroscopy with wavelength modulation: Elimination of residual amplitude modulation in a phasor decomposition approach," Sensors and Actuators B: Chemical **150**, 367–375 (2010).
8. Y. Bidaux, R. Terazzi, A. Bismuto, T. Gresch, S. Blaser, A. Muller, and J. Faist, "Measurements and simulations of the optical gain and anti-reflection coating modal reflectivity in quantum cascade lasers with multiple active region stacks," Journal of Applied Physics **118**, 093101 (2015).
9. A. Bismuto, Y. Bidaux, C. Tardy, R. Terazzi, T. Gresch, J. Wolf, S. Blaser, A. Muller, and J. Faist, "Extended tuning of mid-ir quantum cascade lasers using integrated resistive heaters," Optics Express **23**, 29715 (2015).
10. D. Y. K. Ko and J. R. Sambles, "Scattering matrix method for propagation of radiation in stratified media: attenuated total reflection studies of liquid crystals," JOSA A **5**, 1863–1866 (1988).
11. H. Willenberg, G. H. Döhler, and J. Faist, "Intersubband gain in a Bloch oscillator and quantum cascade laser," Phys. Rev. B **67**, 085315 (2003).

#275016 http://dx.doi.org/10.1364/OE.24.026464
Journal © 2016 Received 31 Aug 2016; revised 14 Oct 2016; accepted 14 Oct 2016; published 7 Nov 2016

Optics EXPRESS

12. R. Terazzi and J. Faist, "A density matrix model of transport and radiation in quantum cascade lasers," New Journal of Physics **12**, 033045 (2010).
13. L. Tombez, F. Cappelli, S. Schilt, G. Di Domenico, S. Bartalini, and D. Hofstetter, "Wavelength tuning and thermal dynamics of continuous-wave mid-infrared distributed feedback quantum cascade lasers," Appl. Phys. Lett. **103**, 031111 (2013).
14. M. Süess, P. Hundt, B. Tuzson, S. Riedi, J. Wolf, R. Peretti, M. Beck, H. Looser, L. Emmenegger, and J. Faist, "Dual-Section DFB-QCLs for Multi-Species Trace Gas Analysis," Photonics **3**, 24 (2016).
15. A. A. Kosterev, Y. A. Bakhirkin, R. F. Curl, and F. K. Tittel, "Quartz-enhanced photoacoustic spectroscopy," Optics Letters **27**, 1902–1904 (2002).
16. P. Patimisco, G. Scamarcio, F. Tittel, and V. Spagnolo, "Quartz-Enhanced Photoacoustic Spectroscopy: A Review," Sensors **14**, 6165–6206 (2014).
17. P. Patimisco, A. Sampaolo, L. Dong, M. Giglio, G. Scamarcio, F. Tittel, and V. Spagnolo, "Analysis of the electro-elastic properties of custom quartz tuning forks for optoacoustic gas sensing," Sensors and Actuators B: Chemical **227**, 539–546 (2016).
18. L. Rothman, I. Gordon, Y. Babikov, A. Barbe, D. Chris Benner, P. Bernath, M. Birk, L. Bizzocchi, V. Boudon, L. Brown, A. Campargue, K. Chance, E. Cohen, L. Coudert, V. Devi, B. Drouin, A. Fayt, J.-M. Flaud, R. Gamache, J. Harrison, J.-M. Hartmann, C. Hill, J. Hodges, D. Jacquemart, A. Jolly, J. Lamouroux, R. Le Roy, G. Li, D. Long, O. Lyulin, C. Mackie, S. Massie, S. Mikhailenko, H. Müller, O. Naumenko, A. Nikitin, J. Orphal, V. Perevalov, A. Perrin, E. Polovtseva, C. Richard, M. Smith, E. Starikova, K. Sung, S. Tashkun, J. Tennyson, G. Toon, V. Tyuterev, and G. Wagner, "The HITRAN2012 molecular spectroscopic database," Journal of Quantitative Spectroscopy and Radiative Transfer **130**, 4–50 (2013).

1. Introduction

Quantum Cascade Lasers (QCL) [1] are mature and reliable coherent semiconductor sources emitting in the mid infrared. Reaching watt-level output power at room temperature [2, 3], exibiting both high performance and low power consumption [4], they are widely used for various applications, such as sensing [5] or countermeasures [6]. In particular, the advent of QCLs triggered the development of tunable laser absorption spectroscopy methods in the mid infrared. In tunable laser absorption spectroscopy, molecular spectra are acquired by scanning a single mode laser source across the selected rotational-vibrational line. This is typically obtained by direct modulation of the laser injection current. However, changing the laser current not only modifies the lasing frequency, but also the output power. Therefore, careful normalization of the signal is required in most cases to remove the residual amplitude modulation (RAM) effect [7]. In this work, we designed a three sections buried heterostructure (BH) single mode QCL allowing non-uniform pumping in the gain, master oscillator (MO) and phase sections (PS). We demonstrated the possibility to achieve independent modulation of the output power and the emission frequency by selectively modulating the injected current in the different laser sections. Pure modulation of the output power is obtained by varying the mirror losses of the laser due to a phase section fabricated close to the device's front facet. To demonstrate the achievement of a pure laser amplitude modulation (AM), we implemented the QCL in a quartz-enhanced photoacoustic sensor (QEPAS) and selected N_2O as the target gas. QEPAS spectral scans, background-free and with nearly perfect Voigt line-shape, were obtained clearly proving the absence of any RAM contribution and the achievement of a pure AM operating condition.

2. Fabrication

A QCL emitting at 7.8 μm was fabricated. The active region design is based on the 2-phonons transition design detailed in one of our previous work [8]. The device was processed to a 6 mm long and 9.5 μm wide buried QCL [9]. The three independent sections were electrically separated by etching 1.5 μm deep in the InP regrowth. The scheme of the device is depicted in Fig. 1.

During the fabrication process a buried grating was defined in the 2.25 mm long back section (Fig. 1, MO). The central gain section is 3.00 mm long and is used to pump the laser gain (Fig. 1, Gain). At the front facet, an additional 0.75 mm PS section was defined in order to control the

Optics EXPRESS

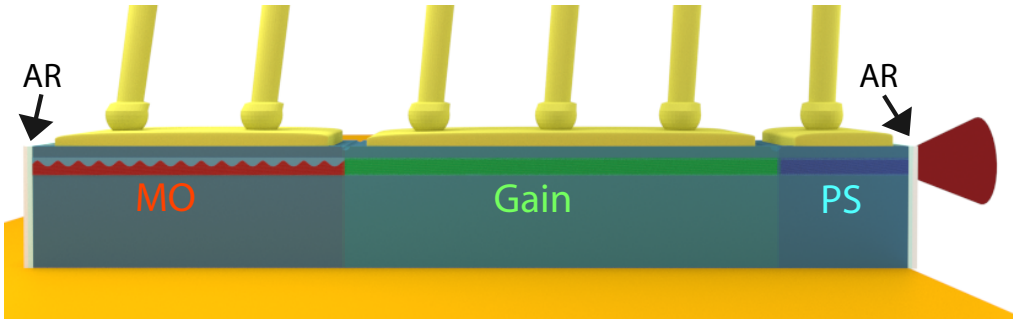

Fig. 1. Schematic view of the device. The device is electrically separated into three sections: Master oscillator (MO, 2.25 mm), Gain (3 mm), Phase section (PS, 0.75 mm). Anti-reflective coating layers were deposited on the device's back and front facets.

facet effective reflectivity by adjusting the reflection phase (see Fig. 1, PS). In order to ensure that the laser operates on the optical mode selected by the MO section, YF_3/ZnSe (0.598/0.250 μm) anti-reflective coatings were deposited on the device's back and front facets. This leads to an increase of the losses of Fabry-Perot modes located between the laser front and back facets and prevents them from lasing. The modal reflectivity of the deposited coating was measured [8] and results are displayed in Fig. 2. A reflectivity as low as 0.1 % is measured at 1278 cm^{-1}.

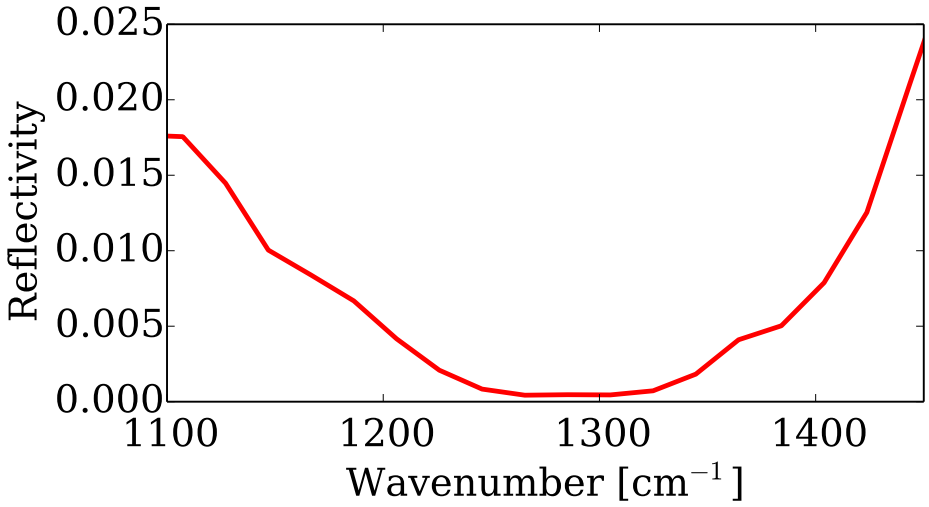

Fig. 2. Measured modal reflectivity of the anti-reflective coating layers deposited on the device's back and front facets, composed of YF_3/ZnSe (0.598/0.250 μm).

3. QCL characterization

To determine the QCL source optical properties, we investigated its light-current characteristics while non-uniform current is injected in the three laser sections. The heat-sink temperature of the QCL was set to -10 °C, 0.8 A were injected in the gain section and the output power and optical spectrum were recorded while varying: the current injected in the MO section in the range 0.42 to 0.57 A (4.5 W to 6.5 W electrical power) and that in the PS section from 0 A to 0.2 A (0 W to

Optics EXPRESS

2.2 W electrical power). The obtained results are displayed in Fig. 3. When the current injected

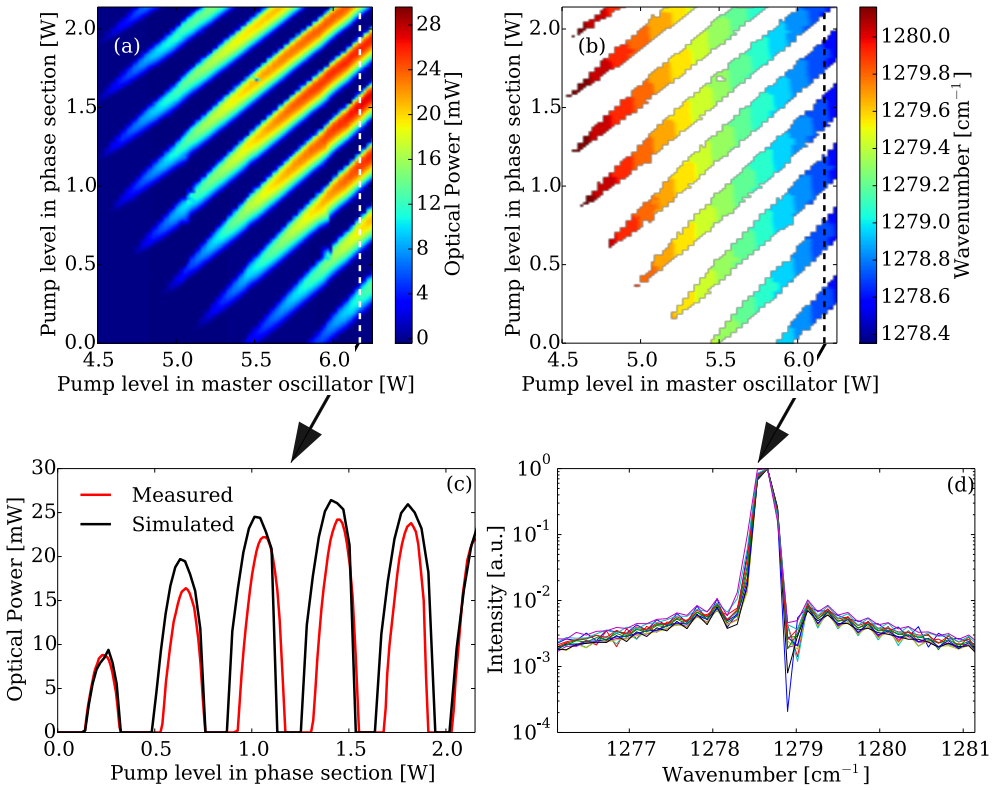

Fig. 3. (a) and (b): QCL output power and emission wavelength measured while varying the electrical power dissipated in the MO section from 4.5 W to 6.5 W (0.42 to 0.57 A MO current) and from 0 W to 2.2 W (0 A to 0.2 A PS current) in the PS section. The heat-sink temperature was set to -10°C. (c) Simulated and measured light current dependency of the QCL at 6.1 W pumped in MO (d) Corresponding spectra: the emission is single mode and no frequency tuning is observed as a function of the PS section current.

in the MO section is varied and the current injected in the PS section is kept constant, the laser emission wavelength is tuned (see Fig. 3(b)). This is due to a temperature tuning of the refractive index, which induces a shift of the grating's Bragg frequency. The total current tuning range achieved reaches 1.7 cm^{-1}. When the current in the PS section is varied while the MO current is kept constant, the emission wavelength remains constant (see Fig. 3(d)). However, while the PS current is ramped up the laser is turned off and on periodically (see Fig. 3(c)). Therefore the PS section can be used as pure amplitude modulator with a depth of modulation of 100% of the available output power. We note that the output power variation versus the PS injected current (2.5 W·A^{-1}) is much higher than that typically observed in standard DFB QCLs (0.6 W·A^{-1} [4]). Because the modulation of the output power is obtained by varying the refractive index in the PS, the bandwidth of such a modulator should be limited by dynamics of thermal processes inside the laser ridge. The bandwidth of the modulation achievable with the PS was measured to be as high as 200 kHz (see Fig. 4) which corresponds to the cut off of thermal dynamics for DFB QCLS [13].

Optics EXPRESS

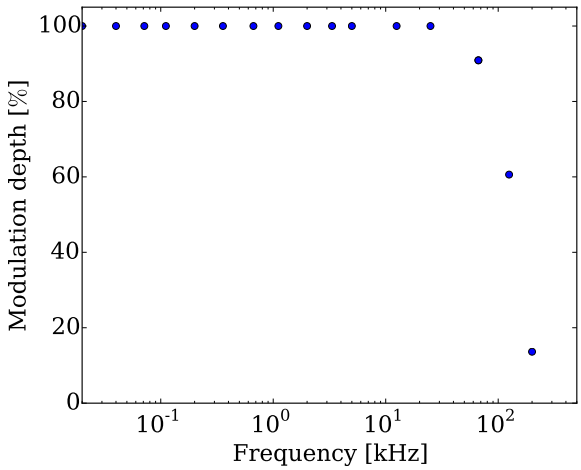

Fig. 4. Modulation depth as a function of the PS modulation frequency. Bandwidth as high as 200 kHz has been achieved, corresponding to the cut off of thermal dynamics for DFB QCLS.

4. Optical field simulation

In order to understand the origin of these emitted power oscillations, we simulated the optical cavity using the scattering matrix formalism [10] whereas the current dependence of the net modal gain for this particular device was measured and simulated using the density matrix formalism [11]. For a fixed current in the gain and MO sections, the current in the PS section is increased. For each current step, the temperature and net modal gain of each laser section was computed as a function of the injected DC current [8] and the value of the refractive indices were changed accordingly. The scattering matrix of the optical cavity was computed and the threshold condition assessed. If the threshold losses are higher than the net modal gain, then the laser output power is zero. If the threshold losses are lower than the net modal gain, then the threshold condition needs to be matched by varying the photon flux S [12]. In order to compute the output power of the multiple section single mode device accurately, the spatially resolved saturation of the pump has to be computed as a function of the highly inhomogeneous mode profile (see Fig. 5). The spatially resolved pump saturation factor d(x,S) is computed using eq. 1.

$$d(x, J) = \frac{1}{1 + \frac{S(x,J)}{S_s}} \tag{1}$$

where S(x,J) is the spatially resolved mode profile at current density J and position x and S_s = $2.6{\cdot}10^{20}$ cm^{-1} s^{-1} is the saturation intensity obtained from our density matrix model [12]. The light current dependence was solved starting with the cold cavity approximation at threshold and then by increasing the current in the PS section. For each subsequent step the mode profile of the previous one was used as initial estimate for the saturation profile. Finally, a self-consistent solution was found by iterating this process until convergence. The light current dependence is displayed in Fig. 3(c) in black and shows a good agreement with measurements. This shows that these oscillations are caused by the modulation of the cavity losses due to the refractive index change in the PS section. Even though the overall laser pump is increased, the variation of the reflection phase at the facets induces an increase of the threshold losses which in turn causes the laser to periodically switch on and off. Such effect was already observed previously [14]. In the present case, the effect is strong even though the residual facet reflectivity is low because a large

Optics EXPRESS

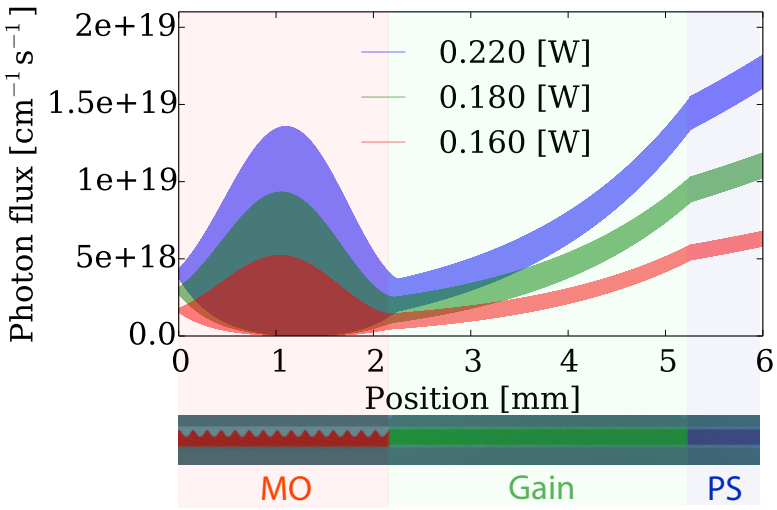

Fig. 5. Simulated spatially resolved mode profile for three different pump levels in the PS section.

gain is present in the gain section.

5. Pure amplitude modulated QEPAS

The particular device capability demonstrated in the last paragraphs can be exploited in tunable-laser spectroscopy for gas detection. A sinusoidal dither applied to the PS will produce a modulation of the QCL output power intensity but not a variation of its wavelength. Simultaneously the gas absorption line can be scanned by adding a slow ramp to the MO current, realizing a pure AM configuration. To verify this assumption we employed one of the most sensitive spectroscopic gas techniques, namely quartz enhanced photoacoustic spectroscopy (QEPAS) [15, 16].

Pure AM modulation has been achieved in standard Photoacoustic (PAS) sensors employing optical choppers. This method cannot be implemented in a QEPAS-based sensor system since QEPAS requires chopping frequencies in the kHz range and commercially available optical choppers in this range have a frequency resolution of 1 Hz, much larger than the bandwidth of the quartz tuning fork resonance. Also, optical choppers are quite noisy, leading to a significant noise contribution to the detected QEPAS signal.

The QEPAS detection module is composed of a custom-made quartz tuning fork (QTF) [17]. The prong of the QTF is 17 mm long, 1 mm wide and 0.25 mm thick. The spacing between the two prongs is 0.7 mm. The QTF is enclosed in a compact, vacuum-tight gas cell equipped with two ZnSe windows with a 3-12 μm AR coating. The pressure inside the cell is kept fixed at 85 Torr. The QCL was placed in a high heat load housing (HHL) including a lens and yielding a parallel beam of 4 mm diameter. The laser beam was focused between the prongs of the QTF using a 1-inch diameter ZnSe lens with 3-12 μm anti-reflection (AR) coating and a focal length of 50 mm (see Fig. 6). The QTF signal was measured using a transimpedance amplifier mounted on a circuit positioned into the gas cell and equipped with an electronic switch allowing electrical excitation of the QTF. This feature was used to determine the main QTF electrical parameters. At a gas pressure of 85 Torr, we measured a resonance frequency f_0 = 2871.76 Hz, an electrical resistance R = 482.5 kΩ and a quality-factor Q = 12400. The electrical signal exiting from the circuit was demodulated by means of a lock-in amplifier. Digitalization of the demodulated signal was performed using a National Instruments DAQ Card and a LabVIEW program was

used to perform the trace gas measurements. QEPAS spectral scans were obtained by measuring the lock-in amplifier signal amplitude at the resonance frequency as a function of time, while the laser center frequency is swept through the selected N_2O absorption line. The time axis was then converted to wavenumbers based on the laser-tuning parameter, previously determined. The lock-in integration time was set to 100 ms for all measurements. To demonstrate the QEPAS sensor operation in pure AM, we selected a N_2O absorption line falling within the QCL operation range and precisely at 1278.96 cm^{-1}, with a line-strength of $1.07 \cdot 10^{-19}$ cm^{-1}/mol. Pure AM technique and $1f$ ($2f$) detection schemes were implemented by applying a sinusoidal dither to PS at f_0 (f_0 /2) and demodulating the QEPAS signal at f_0. The current modulation depth of

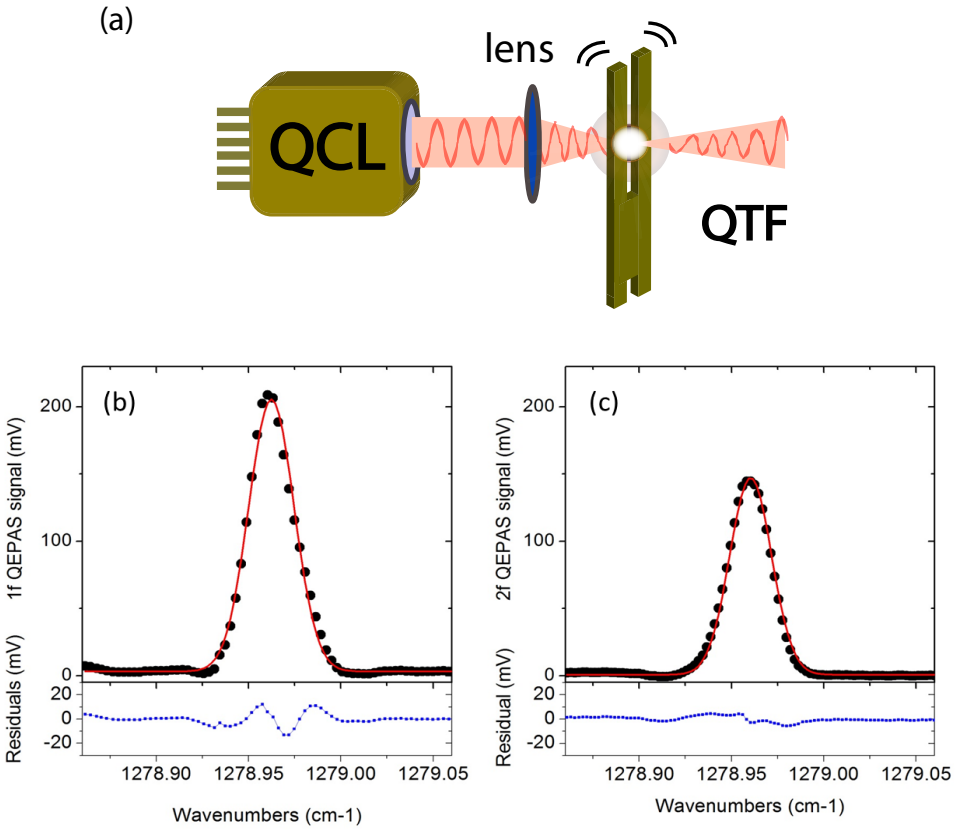

Fig. 6. (a) Schematic of the QCL-QTF optical coupling. Both $1f$ (b) and $2f$ (c) QEPAS spectral scans (black dots) show a background-free Voigt line-shape (red curve), demonstrating the achievement of a pure AM condition. Residuals are depicted in the related lower panels.

the PS section must be carefully selected in order to switch between QCL on and off emission during each oscillation. The resulting effect is that the modulation of the optical power can be approximated by a truncated sine waveform. A Fourier analysis of such a waveform shows that the strongest harmonic components are the fundamental and the second harmonic, while higher harmonics can be neglected. Hence, the optical power modulation can be approximated by:

$$P_{opt} \propto A\cos(2\omega t) + B\cos(\omega t) \tag{2}$$

Optics EXPRESS

If the laser frequency does not change during the PS section modulation, from the Lambert-Beers law the absorbed optical intensity is:

$$I_{abs}(t) = [A\cos(2\omega t) + B\cos(\omega t)]\,[\alpha(\omega)L] \tag{3}$$

where t is the time, ω is the angular frequency, α (ω) is the absorption coefficient, L is the cavity length and A and B are amplitude coefficients of the harmonic components. As a result, both the $1f$ and $2f$ QEPAS signal should exhibit a Lorentzian line-shape. We experimentally determined the modulation depths maximizing the QEPAS signal for $1f$ and $2f$ detection, which result in 23.0 mA and 17.6 mA, respectively. The DC current of PS section was fixed at 110 mA, while a ramp was applied to the MO injected current at a frequency of 20 mHz, scanning from 540 to 558 mA. QEPAS spectral scans obtained at $1f$ and $2f$ detection schemes are reported in Fig. 6(b) and 6(c). The optical power measured at the peak value is 18 mW.

Both QEPAS spectra show a nearly background-free Voigt line-shape, meaning that pressure broadened mechanisms are comparable to Doppler induced broadending effects. For $1f$ detection we measured a linear baseline of 2.63 mV, while for the $2f$detection is 2.15 mV. These baseline levels are comparable with 3σ noise level ($\sim$ 1.2 mV), extracted for $1f$ and $2f$ detection, thus demonstrating that the proposed technique is background-free. The ratio between $1f$-peak value and $2f$-peak value is 1.44, while the FWHM Lorentzian contribution to the Voigt fit for both peak spectra is 0.0267 $\pm$ 0.0007 cm^{-1}, close to the pressure-broadening coefficient of 0.026 cm^{-1} in air for the operating pressure condition, as reported in the HITRAN database [18].

6. Conclusion

In this work we reported an innovative QCL composed of three different sections, each one independently driven. We have demonstrated that by selectively modulating current in the PS section a pure AM operating condition can be reached. We confirmed this achievement using QEPAS spectroscopy as test gas sensing technique and demonstrated that under this AM configuration it is possible to obtain, both in $1f$ and $2f$ operating schemes, background-free spectral scans having Voigt absorption profiles. For these reasons, the proposed technique can be used for gas sensing applications, especially for the detection of broadband absorbers, as well for investigations of absorption linewidth broadening phenomena, such as self-broadening and collision-induced, pressure-dependent broadening in an unrelated matrix.

Funding

Welch Foundation (Grant R4925S); Ministero dellâĂŹIstruzione, dellâĂŹUniversitÃă e della Ricerca (PON02 00675; PON02 00576).

Acknowledgments

We thank Dr. Richard Maulini, Dr. Lorenzo Lugani, Sokratis Papaloukas and Dr. Martin Suess for fruitful discussions and the Alpes Lasers team for technical support. Frank Tittel acknowledges support by the Welch Foundation. The authors from Dipartimento Interateneo di Fisica di Bari acknowledge financial support from two Italian research projects.

193.204.188.118 {ts '2016-11-08 02:52:06'}